Accepted Manuscript

AlTiN based thin films for degradation protection of tetrahedrite thermoelectric material

S. Battiston, F. Montagner, S. Fiameni, A. Famengo, S. Boldrini, A. Ferrario, C. Fanciulli, F. Agresti, M. Fabrizio

PII: S0925-8388(19)31395-7

DOI: https://doi.org/10.1016/j.jallcom.2019.04.116

Reference: JALCOM 50300

To appear in: *Journal of Alloys and Compounds*

Received Date: 17 December 2018

Revised Date: 12 March 2019

Accepted Date: 10 April 2019

Please cite this article as: S. Battiston, F. Montagner, S. Fiameni, A. Famengo, S. Boldrini, A. Ferrario, C. Fanciulli, F. Agresti, M. Fabrizio, AlTiN based thin films for degradation protection of tetrahedrite thermoelectric material, *Journal of Alloys and Compounds* (2019), doi: https://doi.org/10.1016/j.jallcom.2019.04.116.

$Cu_{10.1}Zn_{0.2}Ni_{1.3}Sb_{4.0}S_{13.0}$ after 5 hour air annealing at 450 °C

Without protective coating

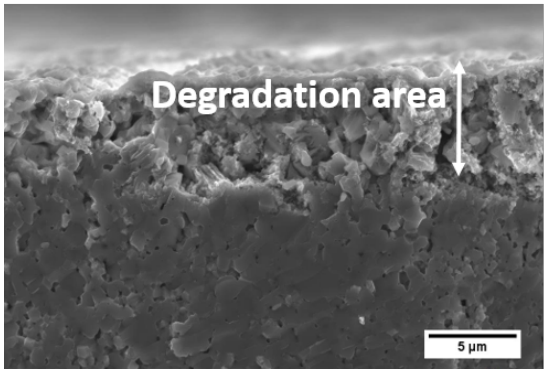

AlTiN film as protective coating

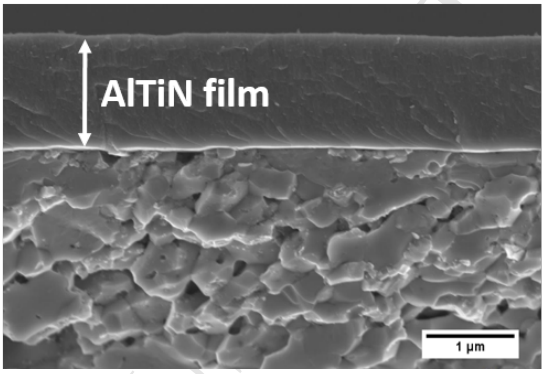

AlTiN based thin films for degradation protection of tetrahedrite thermoelectric material

S. Battiston, F. Montagner, S. Fiameni*, A. Famengo, S. Boldrini, A. Ferrario, C. Fanciulli, F. Agresti, M. Fabrizio

CNR - ICMATE, Corso Stati Uniti 4, 35127 Padova, Italy
CNR - ICMATE, Via Previati 1/E, 23900 Lecco, Italy
stefania.fiameni@cnr.it

Abstract

Efficient protection against degradation process of tetrahedrite-based thermoelectric materials was obtained employing AlTiN based thin films. The coatings were deposited via reactive direct current physical vapour deposition magnetron sputtering. The composition, thermal and electrical behaviour of thin films were investigated by X-ray diffraction, energy dispersive spectroscopy associated to field emission scanning electron microscopy, thermogravimetric analyses and electrical conductivity measurements. The barrier features for oxygen protection during thermal treatment in air at 500 °C were qualitatively evaluated, studying the coating behaviour over the higher operating temperature of tetrahedrite based thermoelectric devices.

Keywords: thermoelectric, tetrahedrite, air stability, AlTiN coating

1. Introduction

In the last years the interest in thermoelectric materials increased mainly due to the possibility of designing thermoelectric generators (TEGs) [1]. TEGs importance becomes evident where the employment of conventional technologies is not suitable to generate electricity from waste heat.
In order to promote a worldwide diffusion of this technology, the identification of efficient thermoelectric materials, which should be inexpensive, easy to synthesize, and comprised of earth-abundant elements is of pivotal issue. Tetrahedrite mineral family ($Cu_{12}Sb_4S_{13}$), which is one of the most widespread sulfosalts on Earth's crust, seems to be an attractive sustainable source for p-type thermoelectric materials. Many studies reported that tetrahedrites are characterized by high figure of merit ZT ($ZT=\alpha^2\rho^{-1}\kappa^{-1}T$, where α is the Seebeck coefficient, ρ the electrical resistivity and κ the

thermal conductivity) with values around unity at 450 °C [2–4]. In the last years, many research works were devoted to the increase of tetrahedrite figure of merit, confirming the significance of this material and obtaining good thermoelectric performances [5–8].

Beside this research aspect, it is important improving the thermoelectric material stability at the typical operating conditions, facing the thermal decomposition and oxidation phenomena, which are detrimental for materials thermoelectric efficiency.

In particular, previous works revealed that tetrahedrite underwent thermal decomposition involving sulphur volatilization above 500 °C in argon flow [5], establishing the typical maximum operative temperature at 450°C. Furthermore, oxidation processes of the tetrahedrite usually occur in air atmosphere [9]. One way to overcome the problem of thermal degradation and consider tetrahedrite-based materials suitable for practical devices, even operating in air atmosphere, could be the material protection with oxidation-resistant thin films.

To the best of the authors' knowledge, attempts to prevent thermal degradation with protective coatings are reported in literature mainly for silicides and skutterudites TE materials. Al_2O_3-coated $Mg_2Si_{0.4}Sn_{0.6}$ exhibited good oxidation resistance at 550°C [10]. A silica-based glass–ceramic was observed to be an effective oxidation-resistant coating for $MnSi_{1.74}$ [11], whilst $MoSi_2$ thin films were deposited on Mg_2Si to avoid material oxidation up to 600 °C [12]. Yttria-stabilized zirconia/titanium coatings on skutterudite-thermoelectric materials were observed to be effective for preventing Sb sublimation, keeping ZT values almost unchanged after material aging [13].

In this work, AlTiN based thin films were deposited by means of reactive direct current (DC) physical vapour deposition (PVD) magnetron sputtering onto tetrahedrite sintered pellets. In particular, this kind of hard coating, when exposed to high temperature (up to 900 °C), presents the formation of dense, high adhesive, and protective Al_2O_3 layer, retarding diffusion processes [14–17].

For their peculiar properties, AlTiN based films are widely used in many industrial field such as wear resistant coating in cutting tools, aero-engine sector, diffusion barriers in integrated circuits and bio-implants [18–22].

2. Material and Methods

2.1. Syntheses

Similarly to what previously reported [8], Ni-Zn substituted tetrahedrite materials were fabricated via solid state reaction of sulphide powder precursors and elemental sulphur with the nominal stoichiometry of $Cu^{(I)}_{10}Cu^{(II)}_{0.5}Ni_1Zn_{0.5}Sb_4S_{13}$. In a typical synthesis batch, CuS (Sigma Aldrich, 100

mesh, purity of 99%), Cu_2S (Sigma Aldrich, 100 mesh), Sb_2S_3 (Sigma Aldrich,), Ni_3S_2 (Sigma Aldrich, 150 mesh, purity of 99.7%), ZnS (Sigma Aldrich, 10 μm, purity of 99.99%), and S (Sigma Aldrich, 100 mesh, purified by sublimation) were mixed in the appropriate stoichiometry in a 250 mL tungsten carbide jar adding WC balls with a ball to powder ratio =10:1 together with 50 mL of n-hexane (Sigma Aldrich 98.5%) as milling medium.

The mixture was processed in a planetary ball mill (Pulverisette 5 Fritsch) at 350 rpm, with 9 milling cycles of 20 min spaced out with pauses of 10 min. Open die pressing process (ODP) [23] was employed for simultaneous synthesis and consolidation of tetrahedrite powders, obtaining samples with size of about 10 cm^2 and thickness of 6 mm. The powders were sealed into a Fe tube (internal diameter 29 mm, wall thickness 1.5 mm) and closed with iron caps under argon atmosphere to prevent possible oxidation of the powders. The composite billet was preheated in a furnace in air at 550 °C (for 7 min) and pressed down to a final thickness of 6 mm. To prevent reactions or contamination of the tetrahedrite phase, a layer of boron nitride was deposited onto the internal surface of the tube. The sample was kept under a load of 20×10^3 kg for 10 min at 485 °C. After the processing, the sample was naturally cooled down to room temperature. The process parameters were set in order to have an overall time of the whole synthesis and sintering processes below 1.5 hours, including the cooling and the sheath removal steps. The obtained pellet was finally cut into several parallelepiped shaped small pellets (3x3x12 mm) polished using abrasive paper up to P4000.

The protective thin films were deposited by reactive DC PVD magnetron sputtering onto doped Si (100) slides (Si-Mat) and tetrahedrite pellets, previously washed in ethanol and isopropanol. Moreover, AlTiN was also deposited on gold sheet for performing thermal analyses. The sputtering process was carried out starting from a base pressure of 5.0×10^{-7} mbar, employing AlTi target (50:50 wt%, 99.9 % pure, 2" diameter, purchased by MaTek), under a total working pressure of 5.3×10^{-3} mbar, composed of a mixture of Ar (99.9997%) with 25% partial pressure of N_2 (99,998%). The substrate-target distance was set at 45 mm. The corresponding deposition rates resulted to be 7.3 and 17.0 nm min^{-1} with fixed powers of 1.5 W cm^{-2} and 3.5 W cm^{-2}, respectively. The depositions were performed maintaining the substrate at room temperature (RT), 300, 350, 400, and 450 °C. Changing the process time, AlTiN film were grown with three different thicknesses: 450, 1300, and 2600 nm.

2.2. Characterizations

The crystalline phases of samples were revealed by X-ray diffraction (XRD) using a Philips PW 3710 X-Ray diffractometer with Bragg-Brentano geometry and a CuKα source (40 kV, 30 mA).

Phase identification on the XRD profiles was carried out employing Match! software (version 3.2.1 70), exploiting inorganic crystal structure database (ICSD, version 2016/1). Rietveld refinements performed through MAUD software [24] on the XRD profiles gave information on phase amounts, crystallite sizes, preferential orientation, lattice parameters and theoretical densities of samples [25]. Preferential orientation was taken into account by means of spherical harmonics method. XRD analyses were performed on ground tetrahedrite pellet powders, air annealed surface tetrahedrite pellets, and AlTiN based coatings with thickness of 2600 nm (for minimizing the interference given by the substrate). The pellet density was estimated through the method of Archimedes exploiting Sartorius analytical balance EO224S PCE equipped with a density kit YDK03.

The morphological and quantitative compositional characterizations were performed by Sigma Zeiss field emission scanning electron microscope (FE-SEM) equipped with Oxford X-Max energy dispersive X-Ray spectroscopy (EDS) system. The EDS point analyses were carried out onto carbon coated polished tetrahedrite samples and AlTiN based films deposited on doped Si (100) at 20 kV accelerating voltage, with acquisition time of 50 s, employing software INCA 4.14 (Oxford Instruments). For these analyses, 2600 nm thick films were deposited onto monocrystalline doped Si slides in order to have a perfectly planar and conductive substrate. Thickness of 2600 nm was chosen in order to make the quantification assessment reliable, avoiding errors due to the surface morphology and for minimizing the influence of the substrate during the analyses. The software was calibrated for quantification referencing the standards to Co optimization standard (99.995%, Alpha Aesar USA, purchased by Astimex Standards). The employed standards for tetrahedrite analyses were: sphalerite ZnS (synthetic, S 32.91 wt%, Fe 0.01 wt%, Zn 67.07 wt%, Sn 0.01 wt%, Cerac Inc. USA), Copper Cu (99.999 wt% Johnson Matthey Chemicals, UK), and Nickel (99.97 wt%, Alpha Aesar, USA) purchased by SPI Supplies, and stibnite Sb_2S_3 (S 28.300 wt%, Sb 71.700 wt%, Cameca standards). Whilst for AlTiN based films, polished AlN sheet (purchased by Goodfellow, CAS 24304005) was employed as standard. The empirical formulas were calculated maintaining the number of S and N atoms fixed to 13 and 1, for tetrahedrite pellets and AlTiN based coatings, respectively [8]. The respective errors were calculated as the standard deviations of the measurements.

The coated tetrahedrite pellets were also observed in operando by FE-SEM during heating in vacuum from RT up to 450 °C employing a heating module (Kammrath & Weiss).

Simultaneous thermogravimetric and differential scanning calorimetry analysis (TG-DSC) were carried out on ground tetrahedrite pellet by means of SDT Q 600 Apparatus (TA Instrument, Waters), with a heating rate of 5 °C/min in air (100 mL/min) from RT to 500 °C. The mass variation of tetrahedrite pellet was investigated as function of time with isothermal analysis at 450

°C for 120 min in air and Ar, in order to evaluate the stability of tetrahedrite at the maximum deposition process temperature.

The mass variation as a function of the temperature of AlTiN films deposited onto Au substrates (Alfa Aesar, 99.997%) was investigated by TGA under air flow (100 mL/min) with a heating rate of 5 °C/min from RT to 500 °C to evaluate the stability of thin film up to the maximum tetrahedrite operating temperature.

The linear shrinkage of ODP sintered tetrahedrite pellets was measured by a dilatometer (Netzsch DIL 402 PC), heating at 5°C/min up to 450 °C under Ar flow (100mL/min) followed by a 60 min of isothermal stage.

Coated and uncoated tetrahedrite pellets and AlTiN based films deposited onto Si slides were treated at 450 °C for 5 h in air, in order to evaluate the possible changes induced by the typical maximum operating temperature of tetrahedrite-based thermoelectric devices (heating rate 10 °C/min, natural cooling).

Electrical conductivity of 2600 nm coating deposited onto an interdigitated electrode Pt/Al_2O_3 (Casa Western Reserve University, US) was measured as a function of the temperature. In particular, the sample was placed at the end of an alumina tube, which was fixed on a stainless steel flange (ProboStat-Norecs, Norway). A S-type thermocouple, Pt wires and gas from the flange were led directly to the sample through alumina tubes.

Pt wires were connected to the interdigitated electrode pads with silver paint. Resistivity measurements were carried out under N_2 atmosphere with 2 °C/min temperature ramp from RT to 400°C by using 2601B source meter unit (Keithley) with 0.1 µA applied current.

3. Results and Discussion

3.1. Tetrahedrite TE material

XRD analyses of the tetrahedrite pellet (figure 1, black line) showed the presence of a single phase (ICSD 62116) with a crystallite size of 2500 nm (2.7 of Rietveld refinement goodness of fit), confirmed by SEM micrograph (figure 2).

The tetrahedrite pellet showed a relative density ≥93%, and its composition was evaluated to be $Cu_{10.1(1)}Ni_{1.3(1)}Zn_{0.2(1)}Sb_{4.0(1)}S_{13.0}$ by EDS quantitative analyses.

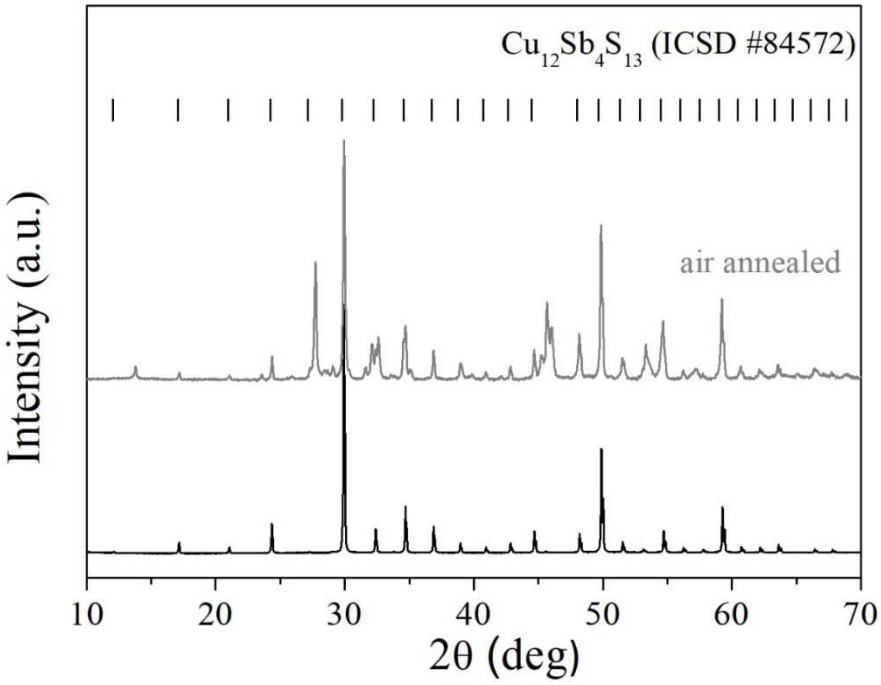

Figure 1: XRD profiles of tetrahedrite ground pellet powder (black line) and tetrahedrite pellet surface after air annealing (grey line). Theoretical peak positions of tetrahedrite are shown in the upper part.

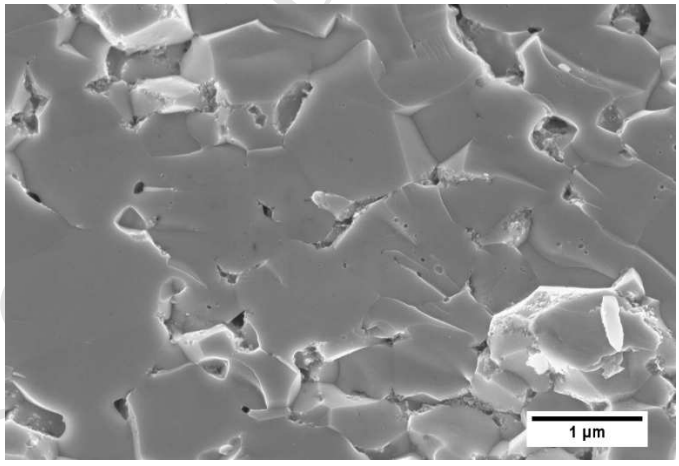

Figure 2: secondary electron micrographs of tetrahedrite pellet surface.

Thermogravimetric analysis was performed on ground pellet powders under air up to 500°C to evaluate the thermal stability of the Ni-Zn substituted synthetic tetrahedrite, as depicted in figure 3. The pellet was ground in order to improve TGA/DSC signal intensities. From 300 °C up to 450 °C a weight gain of about 1% with a corresponding exothermic DSC peak at 384°C were observed, indicating the presence of oxidation processes. A weight loss started at 450 °C, as already reported

in literature [9], with an increase of the DSC signal because of sulphur volatilization process due to thermal decomposition of the tetrahedrite phase.

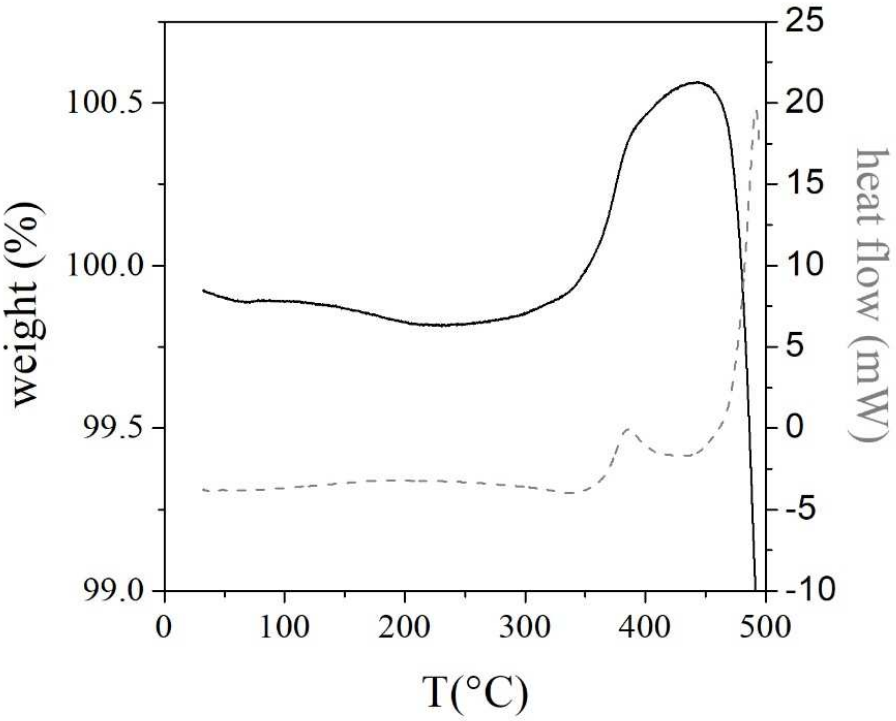

Figure 3: TGA (solid black) and DSC (dash grey) curves for ground pellet of synthetic tetrahedrite under air atmosphere. Exothermic heat flow upwards (5 °C/min).

On the basis of TGA-DSC results, two uncoated tetrahedrite pellets with similar size, were isothermally heated at 450°C for 120 min under argon and air atmosphere, respectively, (figure 4) [8].

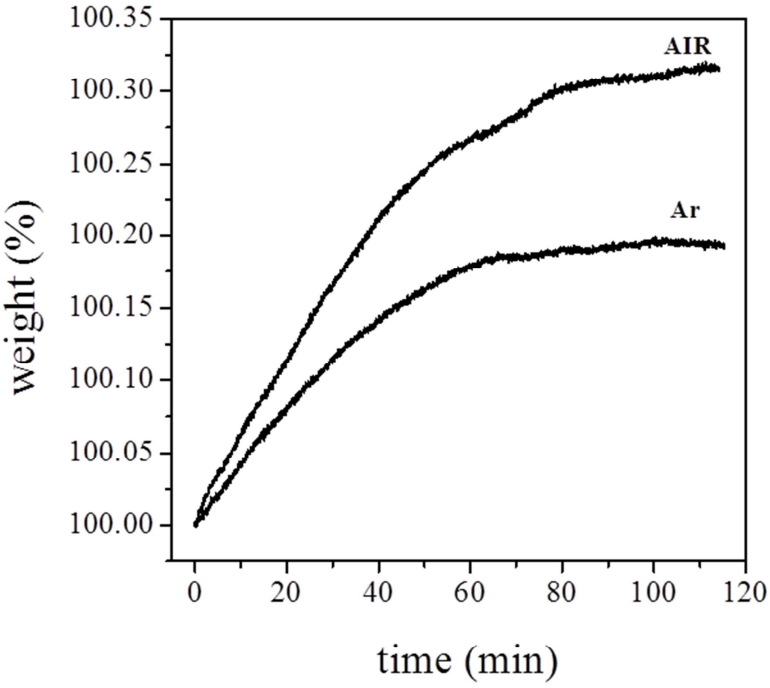

Figure 4: mass variation of two uncoated tetrahedrite sintered pellet isothermally heated at 450°C, under air and argon atmosphere

The sample under Ar showed a total weight increase of 0.19% reaching a plateau from 60 min to the end of measurement. In this case, surface oxidation of the material could be due to oxygen impurities originating from furnace desorption of air at high temperatures. At the beginning of the isothermal heating, the mass gain increased until complete surface passivation (after 60 minutes). Moreover, no sensitive mass losses were detected, indicating that sulphur volatilization is negligible at 450°C for sintered pellets.

Under air atmosphere, a continuous weight gain was observed, reaching a value of 0.32% after 120 minutes. After the measurement under air, the surface of the sample was white, while the color remained unchanged when treated under argon.

Air annealing of the uncoated tetrahedrite pellet was also performed at 450 °C for 5 hours to further investigate its stability behaviour for longer time period. SEM images of annealed sample surface (figure 5a) and the fractured cross section (figure 5b) clearly showed the degradation of material in a sponge-like structure for several microns.

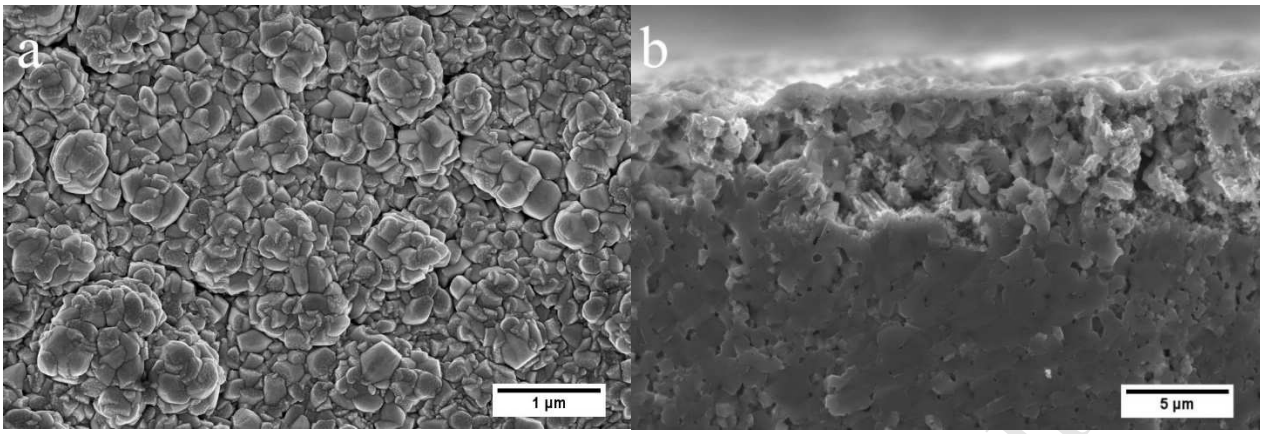

Figure 5: secondary electron micrographs of pellet (a), and pellet cross section (b) after air annealing (450°C for 5 h).

XRD profile of pellet surface after air annealing (grey line) is depicted in figure 1. The identification of the crystallographic phases after the thermal treatment resulted very tricky due to the several peaks of the native tetrahedrite overlapping those of the other new phases. It was possible to recognize the presence of orthorhombic Sb_2O_4 (ICSD 153154), tetragonal $CuSb_2O_6$ (ICSD 84789) and orthorhombic and monocline Cu_3SbS_3 (ICSD 403111 and 81608, respectively). The presence of copper antimony oxide ($CuSb_2O_6$), and antimony tetroxide (Sb_2O_4) is consistent with oxidation process of tetrahedrite-based materials as previously reported in literature [26]. The presence of skinnerite (Cu_3SbS_3) indicated the sulphur volatilization occurred after the sample air annealing.

3.2. AlTiN based coatings

Films deposited at different temperatures did not display substantial morphology differences, showing the typical columnar structure of the thin film deposited with the magnetron sputtering process. As an example, figure 6 shows FE-SEM micrographs of a AlTiN thin film.

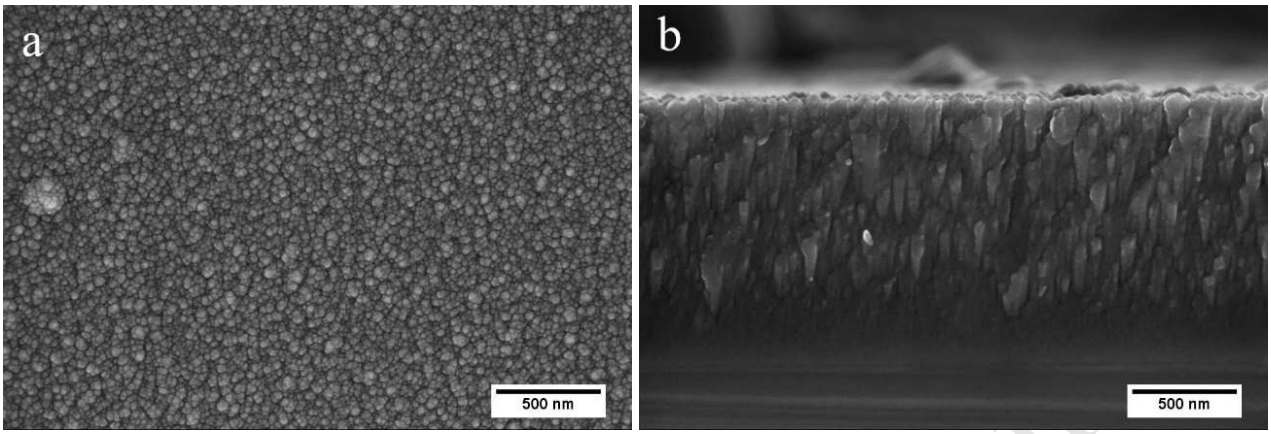

Figure 6: secondary electron micrographs surface (a) and fractured pellet cross section (b) of the AlTiN film deposited onto doped Si at 450°C and 3.5 W cm^{-2}.

EDS analyses of coatings were affected by the Si interdiffusion in the thin films from the substrate, that depends on the different conditions employed for the deposition, such as the temperature of the substrate during the process. For this reason, the most reliable composition assessment can be carried out for the film deposited at RT, which possessed Si content around 1 wt%. Finally, it showed a nitrogen over stoichiometric composition with an empirical formula $Al_{0.61(1)}Ti_{0.24(1)}N_{1.00}$.
The ratio Al/(Al+Ti)=0.65-0.75 is reported to give an idea of the Al maximum solubility level in this kind of material. For the deposited films this ratio reached the value of 0.7, theoretically good enough for having an high Al content to improve the corrosion resistance of the thin film without compromise their mechanical properties [27].
Figure 7 reports the XRD patterns of the AlTiN films (2600 nm thick) deposited onto Si at different substrate temperatures and densities of power. The Rietveld refinement of AlTiN film deposited at RT with 3.5 W cm^{-2} (details are reported in figure 1 of the supplementary materials) highlighted the presence of two AlN-like phases, both derived from the same one (hexagonal p63mc, ICSD 34475). The first phase possessed crystallite size of 30 nm, a preferential orientation of (002) planes parallel to sample plane, and a root mean square (RMS) microstrain of 0.034. Otherwise, the second one resulted even more nanostructured with a high microstrain, meaning a high degree of point defects. In particular, first phase lattice parameters (a: 3.198 Å and c: 5.121 Å) resulted slightly increased if compared with those of pure AlN (a: 3.110 Å and c: 4.980 Å). This behaviour is compatible with a unit cell expansion due to the partial substitution of Al by Ti atoms. This is also corroborated by the absence of Ti-based phases detection.
Increasing the deposition temperature up to 350 °C, the profiles did not change dramatically, and the main peak shifted towards lower angles and became broader. It likely depended on the Ti presence rising in the crystal structure, and on the higher content of highly nanostructured phase.

The latter, in particular, could mainly derive by the deposition rate augment, which is directly related to the nitrogen reaction temperature dependence. In the case of film deposited at 350°C, the effect of the deposition rate was not noticeable resulting 6.6 nm min^{-1}, as in the case of RT deposition. On the contrary, in the case of films deposited at 450°C, the deposition rate increased up to 7.8 nm min^{-1}, leading to the formation of a broad peak centred at further lower angles.

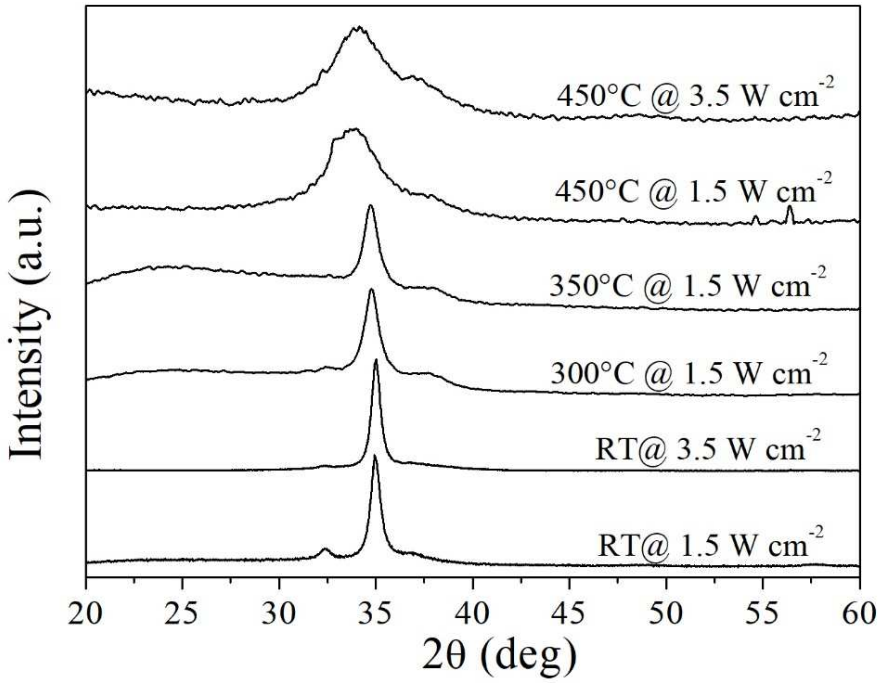

Figure 7: XRD profiles of AlTiN coatings deposited onto Si as a function of deposition temperature and power supplied. For the sake of clarity, the Si-related peak at 33.0° were removed from the profiles, when revealed.

In order to evaluate the effective AlTiN film stability in air atmosphere at typical tetrahedrite operating temperatures, AlTiN films was deposited (at 450 °C and 3.5 W cm^{-2}) on Au sheets and TGA/DSC analyses were performed in air up to 500 °C (figure 2 of supplementary materials). In this temperature range, neither a substantial weight changes nor endothermal or exothermal peaks were observed confirming the high AlTiN stability, as previously reported in literature [15–17].

Therefore, exactly as expected, air annealing at 450°C of AlTiN coatings for 5 hours (figure 8) did not change the composition of the films. It is worth remembering that the possible passivation layer cannot give rise to revealable diffraction peaks because too thin. Nevertheless, AlTiN coating crystal structures resulted affected by this thermal treatment. In particular, the crystalline phase of the film deposited at RT changed its preferential orientation mainly towards (110) and a lesser extent to (100), with c parameter lengthened to 5.126 Å. The crystallite size substantially did not

change but the RMS microstrain decreased to 0.002, which means fewer point defects of the crystal structure. The Rietveld refinement details are reported in figure 3 of the supplementary materials. Even the film crystalline structure of deposited film at 450 °C was affected by the thermal treatment presenting sharper peaks, more similar to those possessed by the films deposited at 300 and 350°C.

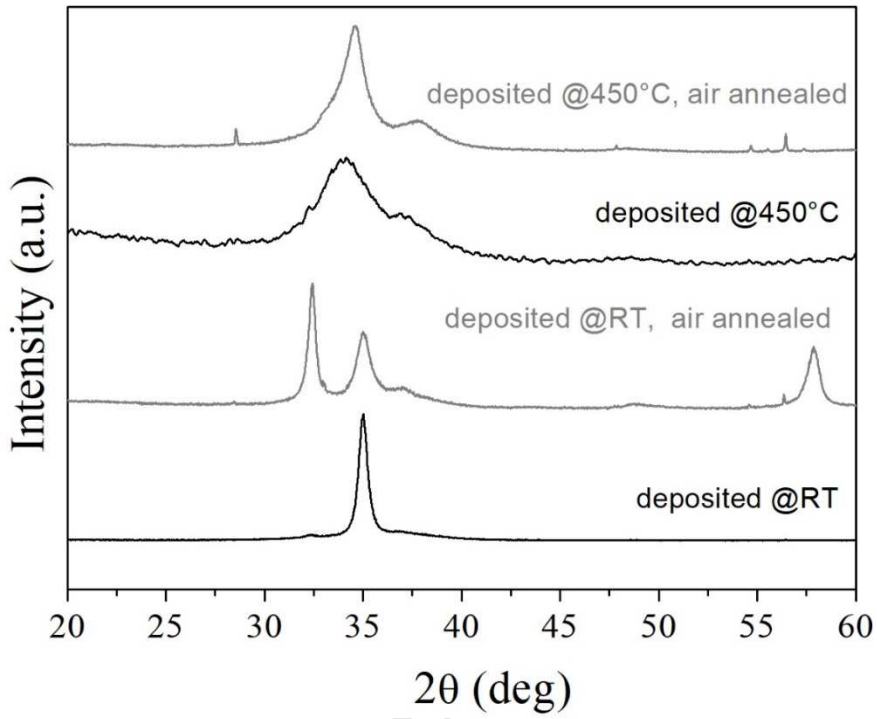

Figure 8: XRD profiles of AlTiN coatings deposited onto doped Si with 3.5 W cm^{-2} at RT and 450°C prior (black lines) and after (grey lines) air annealing. For the sake of clarity, the Si-related peak at 33.0° were removed from the profiles, when revealed.

FE-SEM analyses of AlTiN coatings deposited onto tetrahedrite substrates at RT (with thicknesses of 450, 1300, and 2600 nm) and 450 °C (with thicknesses of 1300 and 2600 nm) were performed in operando up to 450 °C. This characterization highlighted a mechanical failure only for 2600 nm thick film deposited at RT, which completely spalled as soon as it cooled down at RT after the heat treatment. Otherwise, no cracks were observed for any other analysed samples, suggesting a sufficient thermo-mechanical compatibility between the AlTiN coatings (CTE of AlTiN film 7.5×10^{-6} °C^{-1} at room temperature [28]) and the tetrahedrite substrate (CTE 15×10^{-6} °C^{-1} between 20 and 400 °C).

The same samples were also air annealed at 450 °C for 5 h, in order to preliminarily test if the coating could be effective in operative temperature condition in harsh atmosphere. After thermal treatment, the films deposited at 450 °C showed a wide spalling process. The 1300 nm thick film

deposited at RT, diversely, showed some cracks where oxidation products (bright zones in figure 9 a) can be observable. Nevertheless, where the film was continuous, it protected the substrate, which resulted intact (figure 9 b).

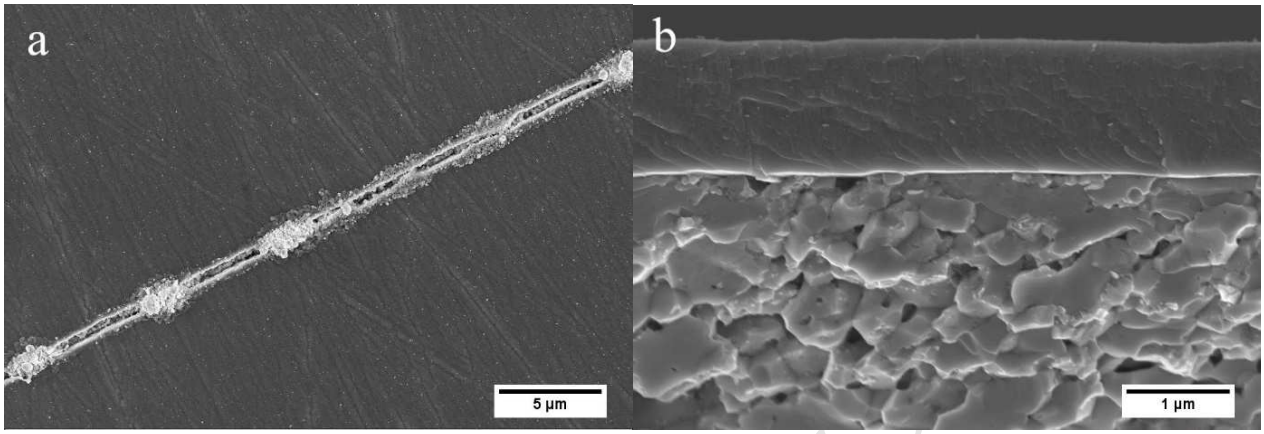

Figure 9: secondary electron micrographs of surface (a) and fractured pellet cross section (b) of the 1300 nm thick AlTiN film deposited onto tetrahedrite at RT after air annealing. The bright zones in figure a are oxidation products occurred along film cracks.

Finally, the 450 nm thick film resulted to have the best performance during the air annealing, resulting to be thick enough to preserve the substrate from the oxidation process, not giving rise to the formation of cracks (figure 10).

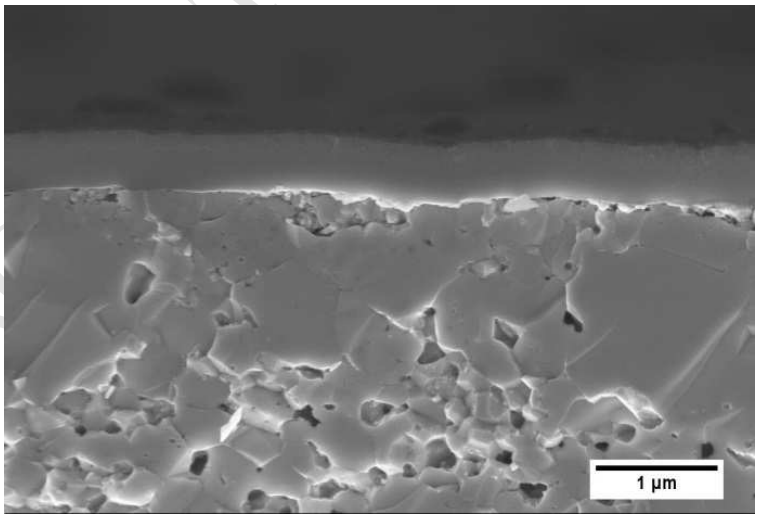

Figure 10: secondary electron micrographs of surface fractured pellet cross section of the 450 nm thick AlTiN film deposited at RT onto doped tetrahedrite and 3.5 W cm^{-2} after air annealing.

Figure 11 reports the resistivity of a 450 nm thick film compared to those of a typical tetrahedrite substrate values [8]. It is worth noting how the difference between the resistivity values of the tetrahedrite substrate and the protective coating resulted roughly 8 order of magnitude at RT and 5 at 400°C. Such resistivity difference, combined with geometry considerations, demonstrate the ability of a 450 nm thick film to avoid any parasitic electrical contribution, maintaining the difference of electric potential between the cold and hot side of the thermoelectric element.

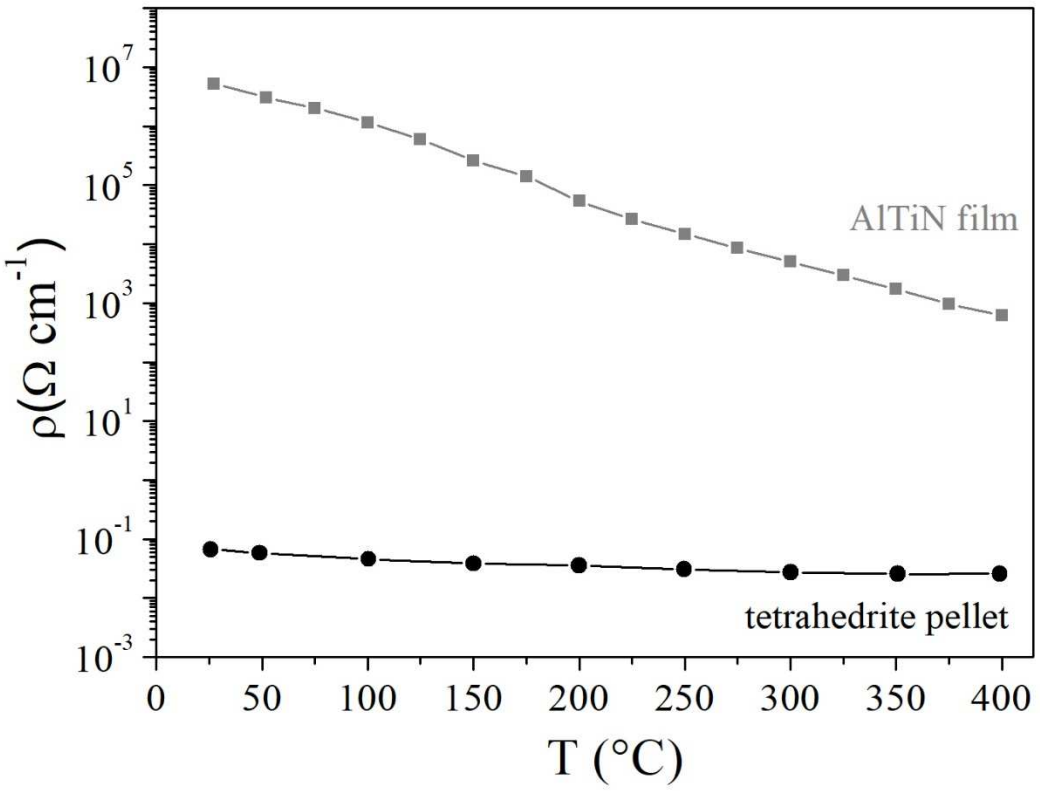

Figure 11: resistivity of a tetrahedrite pellet (black points) compared with the AlTiN film (450 nm, deposited at RT) one (grey points).

Similarly to what discussed regarding the resistivity issue, even the thermal conductivity difference should be taken into account for a qualitative evaluation of the thermoelectric efficiency of the whole coated thermoelectric element. In general, the tetrahedrite thermal conductivity values can vary between about 0.3 and 0.5 W m^{-1} K^{-1} [8], whilst the coating between 5 and 10 W m^{-1} K^{-1} [29–31]. In particular, exploiting the most unfavourable values of those thermal conductivities, a 450 nm film contribute to the whole thermoelectric element thermal conductance would result to be about 3%, for a 2 mm side pellet, typical for a thermoelectric module [32]. It is worth nothing that, due to the typical columnar morphology of the thin film deposited by PVD magnetron sputtering, the value

assumed for the thermal conductivity can be considered an upper limit, restating its secondary role on whole thermal transport.

4. Conclusion

The compatibility of AlTiN protective coatings deposited onto tetrahedrite thermoelectric material was studied. The substrate was characterized by the point of view of crystalline structure, morphology and composition. The composition of the film was chosen in order to maximize the resistance to oxidative environment, increasing the content of Al in the composition. The work highlighted as the layer was effective against oxidation up to 450 °C for 5 hours, when the thickness was lower than 1 µm and the deposition was carried out at RT. The mismatch between the mechanical properties of the layer and the substrate was likely due mainly to the internal stresses created during the deposition processes. The low thickness of the protective coating can help that mechanical compatibility but, in the other hand, make the process of substrate surface polishing very crucial for obtaining the deposition of a continuous and effective protection layer against the harsh atmosphere. Finally, the coating demonstrated to possess the electrical and thermal conductivity features adapt for voiding electrical short circuit phenomena and the heat flux increasing between the hot and cold side, mandatory for maintaining the whole thermoelectric element efficiency as higher as possible.

Acknowledgments

The authors are grateful to the CNR-ICMATE colleagues Silvia Deambrosis and Enrico Miorin for the valuable discussion about the results, and to Enrico Bassani and Stefano Fasolin for his essential technical supports.

This work has been funded by the Italian National Research Council - Italian Ministry of Economic Development Agreement “Ricerca di sistema elettrico nazionale”.

References

[1] S. LeBlanc, Thermoelectric generators: Linking material properties and systems engineering for waste heat recovery applications, Sustain. Mater. Technol. 1–2 (2014) 26–35. doi:10.1016/J.SUSMAT.2014.11.002.

[2] X. Lu, D.T. Morelli, Natural mineral tetrahedrite as a direct source of thermoelectric materials., Phys. Chem. Chem. Phys. 15 (2013) 5762–5766. doi:10.1039/c3cp50920f.

[3] X. Lu, D. Morelli, The effect of Te substitution for sb on thermoelectric properties of tetrahedrite, J. Electron. Mater. 43 (2014) 1983–1987.

http://www.scopus.com/inward/record.url?eid=2-s2.0-84901950320&partnerID=40&md5=9a0291416baf2074abf98e34ef88dea0.

[4] J. Wang, M. Gu, Y. Bao, X. Li, L. Chen, Quick Fabrication and Thermoelectric Properties of Cu12Sb4S13 Tetrahedrite, J. Electron. Mater. 45 (2016) 2274–2277. doi:10.1007/s11664-015-4301-8.

[5] T. Barbier, P. Lemoine, S. Gascoin, O.I. Lebedev, A. Kaltzoglou, P. Vaqueiro, A. V. Powell, R.I. Smith, E. Guilmeau, Structural stability of the synthetic thermoelectric ternary and nickel-substituted tetrahedrite phases, J. Alloys Compd. 634 (2015) 253–262. doi:10.1016/j.jallcom.2015.02.045.

[6] E. Guilmeau, A. Maignan, C. Wan, K. Koumoto, K. Koumoto, T.M. Tritt, M. Kondo, K. Koga, K. Yabuki, G.J. Snyder, R.G. Yang, K. Koumoto, On the effects of substitution, intercalation, non-stoichiometry and block layer concept in TiS_2 based thermoelectrics, Phys. Chem. Chem. Phys. 17 (2015) 24541–24555. doi:10.1039/C5CP01795E.

[7] T. Barbier, P. Lemoine, S. Martinet, M. Eriksson, M. Gilmas, E. Hug, G. Guélou, P. Vaqueiro, A. V. Powell, E. Guilmeau, Up-scaled synthesis process of sulphur-based thermoelectric materials, RSC Adv. 6 (2016) 10044–10053. doi:10.1039/C5RA23218J.

[8] S. Battiston, C. Fanciulli, S. Fiameni, A. Famengo, S. Fasolin, M. Fabrizio, One step synthesis and sintering of Ni and Zn substituted tetrahedrite as thermoelectric material, J. Alloys Compd. 702 (2017) 75–83. doi:10.1016/j.jallcom.2017.01.187.

[9] A.P. Gonçalves, E.B. Lopes, M.F. Montemor, J. Monnier, B. Lenoir, Oxidation Studies of Cu12Sb3.9Bi0.1S10Se3 Tetrahedrite, J. Electron. Mater. 47 (2018) 2880–2889. doi:10.1007/s11664-018-6141-9.

[10] L. Zhang, X. Chen, Y. Tang, L. Shi, G.J. Snyder, J.B. Goodenough Ac, J. Zhou, Thermal stability of Mg 2 Si 0.4 Sn 0.6 in inert gases and atomic-layer-deposited Al 2 O 3 thin film as a protective coating, (2016). doi:10.1039/c6ta07611d.

[11] H. Ning, M.J. Reece, F. Smeacetto, M. Salvo, Oxidation protective glass–ceramic coating for higher manganese silicide thermoelectrics, J. Mater. Sci. 51 (2016) 9484–9489. doi:10.1007/s10853-016-0192-1.

[12] S. Battiston, S. Boldrini, S. Fiameni, A. Famengo, M. Fabrizio, S. Barison, Multilayered thin films for oxidation protection of Mg2Si thermoelectric material at middle-high temperatures, Thin Solid Films. 526 (2012) 150–154. doi:10.1016/j.tsf.2012.10.114.

[13] D. Zhao, D. Wu, J. Ning, M. Zuo, Protective Properties of Various Coatings on CoSb3 Thermoelectric Material, J. Electron. Mater. 46 (2017) 3036–3042. doi:10.1007/s11664-016-5141-x.

[14] F. Vaz, L. Rebouta, M. Andritschky, M.F. da Silva, J.C. Soares, Thermal oxidation of Ti1 − xAlxN coatings in air, J. Eur. Ceram. Soc. 17 (1997) 1971–1977. doi:10.1016/S0955-2219(97)00050-2.

[15] E. Schaffer, G. Klee, Mechanical behavior of Ti,Al N coatings exposed to elevated temperatures and an oxidative environment, Surf. Coatings Technol. 133 (2000) 215–219.

[16] L. Chen, Y. Du, F. Yin, J. Li, Mechanical properties of (Ti, Al)N monolayer and TiN/(Ti, Al)N multilayer coatings, Int. J. Refract. Met. Hard Mater. 25 (2007) 72–76. doi:10.1016/j.ijrmhm.2006.01.005.

[17] L. Chen, Y. Du, X. Xiong, K.K. Chang, M.J. Wu, Improved properties of Ti-Al-N coating by multilayer structure, Int. J. Refract. Met. Hard Mater. 29 (2011) 681–685. doi:10.1016/j.ijrmhm.2011.05.001.

[18] R. Gago, F. Soldera, R. Hübner, J. Lehmann, F. Munnik, L. Vázquez, A. Redondo-Cubero, J.L. Endrino, X-ray absorption near-edge structure of hexagonal ternary phases in sputter-deposited TiAlN films, (2013). doi:10.1016/j.jallcom.2013.01.130.

[19] K. Chakrabarti, J.J. Jeong, S.K. Hwang, Y.C. Yoo, C.M. Lee, Effects of nitrogen flow rates on the growth morphology of TiAlN films prepared by an rf-reactive sputtering technique, Thin Solid Films. 406 (2002) 159–163.

[20] S. Paldey, S.C. Deevi, Single layer and multilayer wear resistant coatings of (Ti,Al)N: a review, Mater. Sci. Eng. A. 342 (2003) 58–79.

[21] S.M. Deambrosis, F. Montagner, V. Zin, M. Fabrizio, C. Badini, E. Padovano, M. Sebastiani, E. Bemporad, K. Brunelli, E. Miorin, Ti1−xAlxN coatings by Reactive High Power Impulse Magnetron Sputtering: film/substrate interface effect on residual stress and high temperature oxidation, Surf. Coatings Technol. 354 (2018) 56–65. doi:10.1016/J.SURFCOAT.2018.09.004.

[22] B. Subramanian, C. V. Muraleedharan, R. Ananthakumar, M. Jayachandran, A comparative study of titanium nitride (TiN), titanium oxy nitride (TiON) and titanium aluminum nitride (TiAlN), as surface coatings for bio implants, Surf. Coatings Technol. (2011). doi:10.1016/j.surfcoat.2011.05.004.

[23] S. Ceresara, C. Fanciulli, F. Passaretti, D. Vasilevskiy, Texturing of (Bi0.2Sb0.8)2Te3 nanopowders by open die pressing, J. Electron. Mater. 42 (2013) 1529–1534. doi:10.1007/s11664-012-2313-1.

[24] L. Lutterotti, S. Matthies, H.R. Wenk, A.S. Schultz, J.W. Richardson Jr, Combined texture and structure analysis of deformed limestone from time-of-flight neutron diffraction spectra, J. Appl. Phys. 81 (1997) 594. doi:10.1063/1.364220.

[25] L. Lutterotti, D. Chateigner, S. Ferrari, J. Ricote, Texture, residual stress and structural analysis of thin films using a combined X-ray analysis, Thin Solid Films. 450 (2004) 34–41. doi:10.1016/j.tsf.2003.10.150.

[26] A.P. Gonçalves, E.B. Lopes, J. Monnier, J. Bourgon, J.B. Vaney, A. Piarristeguy, A. Pradel, B. Lenoir, G. Delaizir, M.F.C. Pereira, E. Alleno, C. Godart, Fast and scalable preparation of tetrahedrite for thermoelectrics via glass crystallization, J. Alloys Compd. 664 (2016) 209–217. doi:10.1016/j.jallcom.2015.12.213.

[27] Q.-X. Fan, T.-G. Wang, Y.-M. Liu, Z.-H. Wu, T. Zhang, T. Li, Z.-B. Yang, Microstructure and Corrosion Resistance of the AlTiN Coating Deposited by Arc Ion Plating, Acta Metall. Sin. (English Lett. 29 (2016) 1119–1126. doi:10.1007/s40195-016-0497-8.

[28] S. Jeon, C.J. Van Tyne, H. Lee, Degradation of TiAlN coatings by the accelerated life test using pulsed laser ablation, Ceram. Int. 40 (2014) 8677–8685. doi:10.1016/J.CERAMINT.2014.01.085.

[29] W. Kalss, A. Reiter, V. Derflinger, C. Gey, J.L. Endrino, Modern coatings in high performance cutting applications, Int. J. Refract. Met. Hard Mater. 24 (2006) 399–404. doi:10.1016/J.IJRMHM.2005.11.005.

[30] M.K. Samani, X.Z. Ding, N. Khosravian, B. Amin-Ahmadi, Y. Yi, G. Chen, E.C. Neyts, A. Bogaerts, B.K. Tay, Thermal conductivity of titanium nitride/titanium aluminum nitride multilayer coatings deposited by lateral rotating cathode arc, Thin Solid Films. 578 (2015) 133–138. doi:10.1016/j.tsf.2015.02.032.

[31] X.Z. Ding, M.K. Samani, G. Chen, Thermal conductivity of PVD TiAlN films using pulsed photothermal reflectance technique, Appl. Phys. A Mater. Sci. Process. 101 (2010) 573–577. doi:10.1007/s00339-010-5900-0.

[32] J.R. Salvador, J.Y. Cho, Z. Ye, J.E. Moczygemba, A.J. Thompson, J.W. Sharp, J.D. Koenig, R. Maloney, T. Thompson, J. Sakamoto, H. Wang, A.A. Wereszczak, Conversion efficiency of skutterudite-based thermoelectric modules, Phys. Chem. Chem. Phys. 16 (2014) 12510–12520. doi:10.1039/c4cp01582g.

Highlights

- Improving the thermal and the structural stability of tetrahedrite based thermoelectric material.
- AlTiN based coatings were deposited via reactive DC PVD magnetron sputtering
- Annealing treatment confirmed tetrahedrite stability due to AlTiN coating